Supplementary Materials and Methods:

Permutation tests (R script):

The functions takes 4 arguments: a vector (*x*) containing all the angular observations; a vector (*subject*) of the same length that specifies from which mouse each observation comes from; another vector (*Group*) of the same length that specifies to which group the mouse belongs; and finally the number (*B*) of permutations to be run to calculate the p-value. Note: Install the R package 'circular' (https://www.rdocumentation.org/packages/circular.) before running tests.

To test changes in mean orientation:

```
angular.meanG.test<-function(x,subject,Group,B)
{
  m<-length(x)
  s<-levels(as.factor(subject))
  ns<-length(levels(as.factor(subject[Group==levels(as.factor(Group))[1]])))
  observed<-abs(mean.circular(x[Group==levels(as.factor(Group))[1]])-
mean.circular(x[Group!=levels(as.factor(Group))[1]]))
  differenza<-NULL
  for(i in 1:B)
  {
    bs<-sample(s,length(s),replace=F)
    sx<-bs[1:ns]
    group1<-x[subject %in% sx]
    group2<-x[subject %in% bs[-c(1:ns)]]
    differenza<-c(differenza,abs(mean.circular(group1)-mean.circular(group2)))
  }
```

```
  return((sum(differenza>observed)+1)/(B+1))

}
```

To test changes in variance:

```
angular.IntraVarG.test<-function(x,subject,Group,B)

{

  m<-length(x)

  s<-levels(as.factor(subject))

  ms<-tapply(x,as.factor(subject),mean.circular)

  cx<-x

  for(i in 1:length(s))

   { cx[subject==s[i]]<-x[subject==s[i]]-ms[i]

    }

  ns<-length(levels(as.factor(subject[Group==levels(as.factor(Group))[1]])))

  observed<-abs(var.circular(cx[Group==levels(as.factor(Group))[1]])-
var.circular(cx[Group!=levels(as.factor(Group))[1]]))

  diff<-NULL

  for(i in 1:B)

  {

    bs<-sample(s,length(s),replace=F)

    sx<-bs[1:ns]

    group1<-cx[subject %in% sx]

    group2<-cx[subject %in% bs[-c(1:ns)]]

    diff<-c(diff,abs(var.circular(group1)-var.circular(group2)))

  }
```

Figure S1

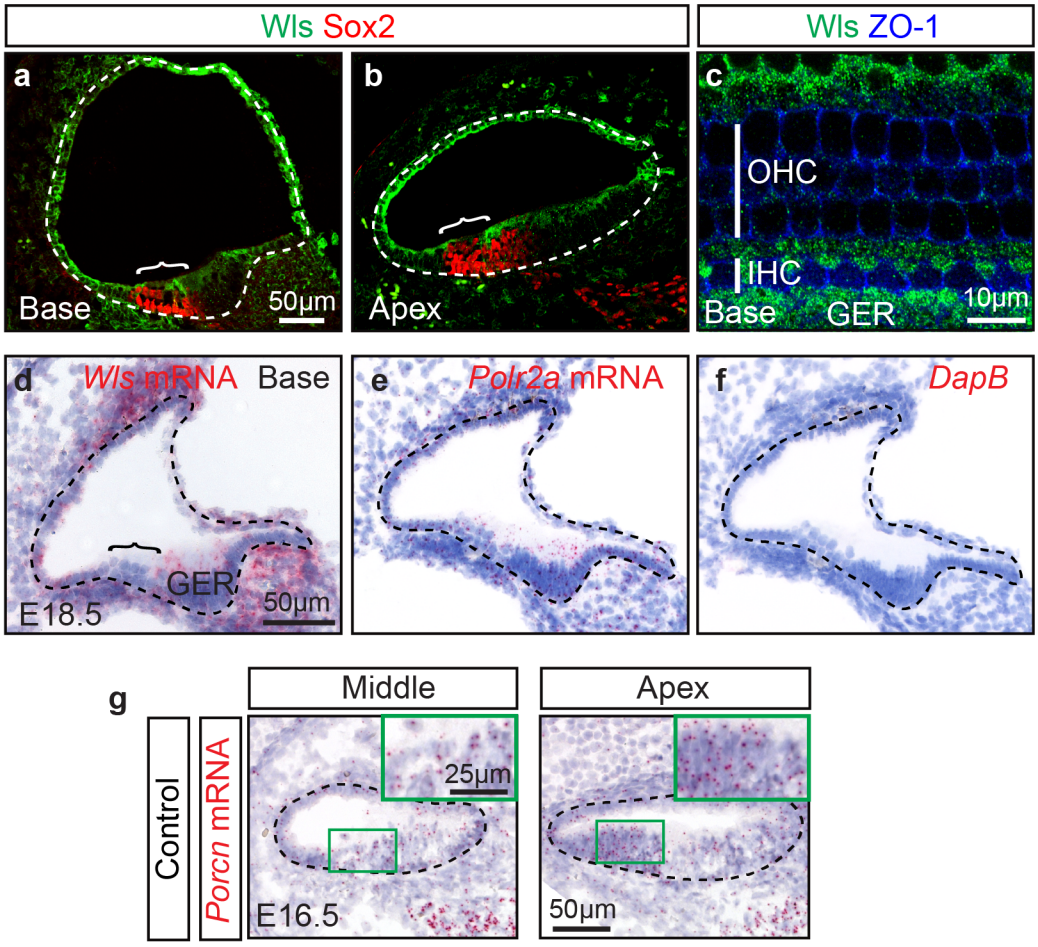

Figure S1. Expression of *Wntless* (*Wls*) and *Porcupine* (*Porcn)* in the embryonic cochlea. (a-b) Sections of E18.5 cochlea showing expression of Wls protein in the basal and apical turns. Sox2 marks hair cells and supporting cells in the organ of Corti. c) Whole mount preparation of E18.5 cochlea immunostained for Wls and the junctional marker ZO-1. At this age, Wls expression was detected primarily in supporting cells in the organ of Corti. d) *Wls* mRNA expression within and outside the E18.5 cochlear duct. (e-f) Positive (*Polr2a*) and negative (*DapB*) control *in situ* hybridization experiments on E18.5 cochlea. (g) *Porcn* mRNA was also detected inside the E16.5 cochlear duct. Hematoxylin staining was used as a counterstain in (d-g). Dashed lines and brackets highlight the cochlear duct and organ of Corti, respectively. OHC=outer hair cells, IHC=inner hair cells, GER= greater epithelial ridge. Each experiment was repeated at least three times on wild type cochleae.

Figure S2

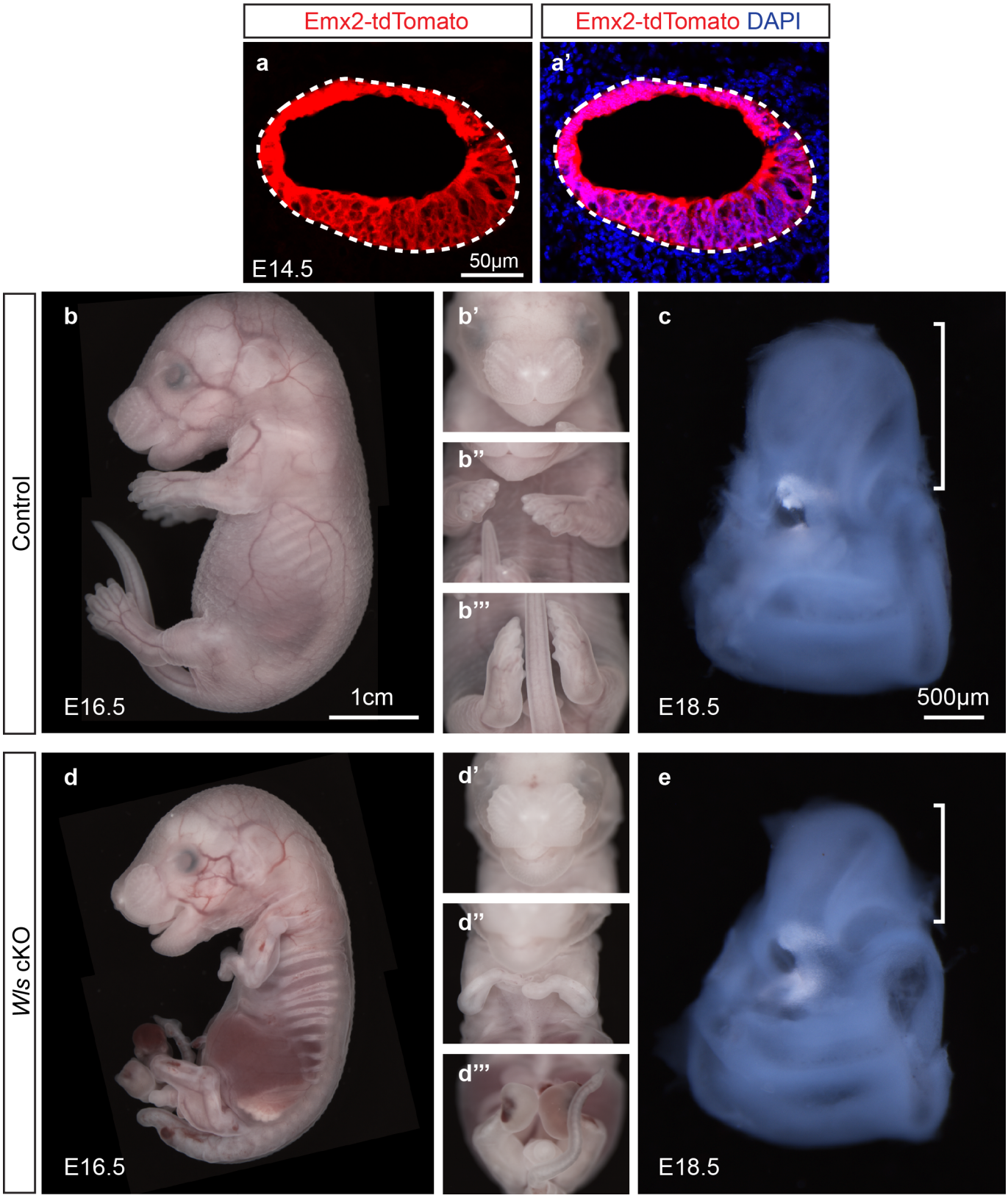

Figure S2. Morphological abnormalities in *Wls* cKO embryos. (a) E14.5 cochlea from *Emx2*$^{Cre/+}$*; Rosa26*$^{tdTomato/+}$ mice. Robust tdTomato expression was detected inside the cochlear duct (marked by dashed lines). DAPI (blue) was used to label nuclei. (b) E16.5 control embryos (*Emx2*$^{Cre/+}$*; Wls*$^{+/fl}$). Ventral view of the head (b'), upper limbs (b'') and lower limbs (b'''). (c) Otic capsule from E18.5 control embryos. Bracket marks the cochlea. (d) E16.5 *Wls* cKO embryos (*Emx2*$^{Cre/+}$*; Wls*$^{fl/fl}$) showing craniofacial defects (d'), and underdeveloped upper (d'') and lower (d''') limbs. (e) Otic capsule of E18.5 *Wls* cKO displaying a short cochlea. Three control and *Wls* cKO animals were analyzed.

Figure S3

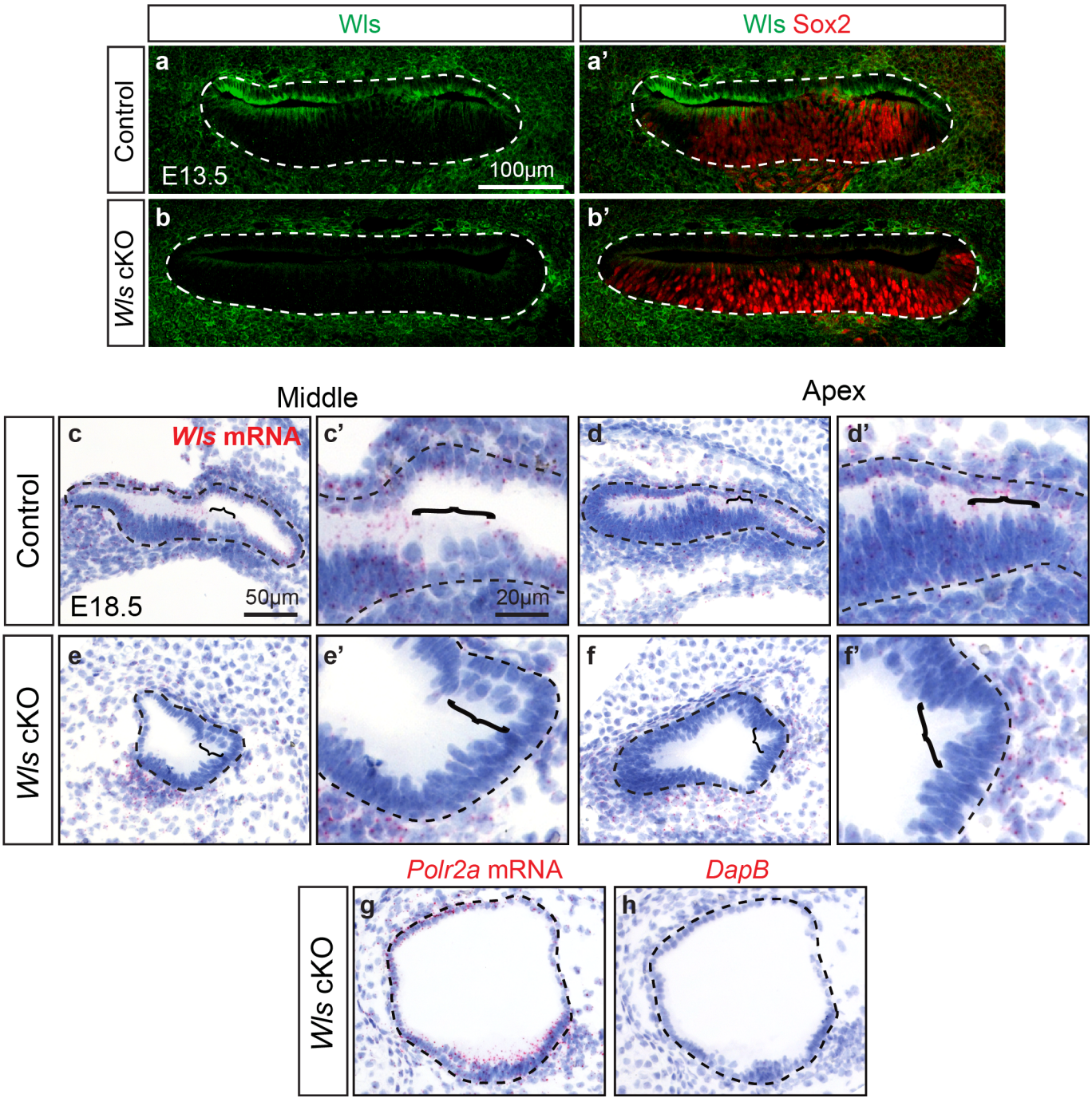

Figure S3. Ablation of *Wls* from the embryonic cochlear duct. (a-b) Cochlear sections from E13.5 control cochlea (*Emx2*$^{Cre/+}$*; Wls*$^{+/fl}$), displaying Wls immunofluorescence in the cochlear duct. In contrast, *Wls* expression was absent in the cochlear duct of *Wls* cKO (*Emx2*$^{Cre/+}$*; Wls*$^{fl/fl}$) mice. Of note, *Wls* expression was detected outside the duct in both control and *Wls* cKO cochleae. The prosensory marker Sox2 was present in both control and *Wls* cKO cochleae. (c-f) *Wls in situ* hybridization in sections from the middle and apical turns of E18.5 control and *Wls* cKO cochleae. *Wls* mRNA was detected in the control cochlea but absent in *Wls* cKO cochlear duct. Higher magnification images of the organ of Corti (marked by brackets) are shown in (c', d', e' and f'). See Supplementary Figure 5 for location of the organ of Corti in *Wls* cKO cochlea. (g-h) Positive (*Polr2a*) and negative (*DapB*) control probes are shown in *Wls* cKO cochlear tissues, respectively. Dashed lines demark the cochlear duct. Hematoxylin (blue) was used to label nuclei. Each experiment was repeated at least three times.

Figure S4

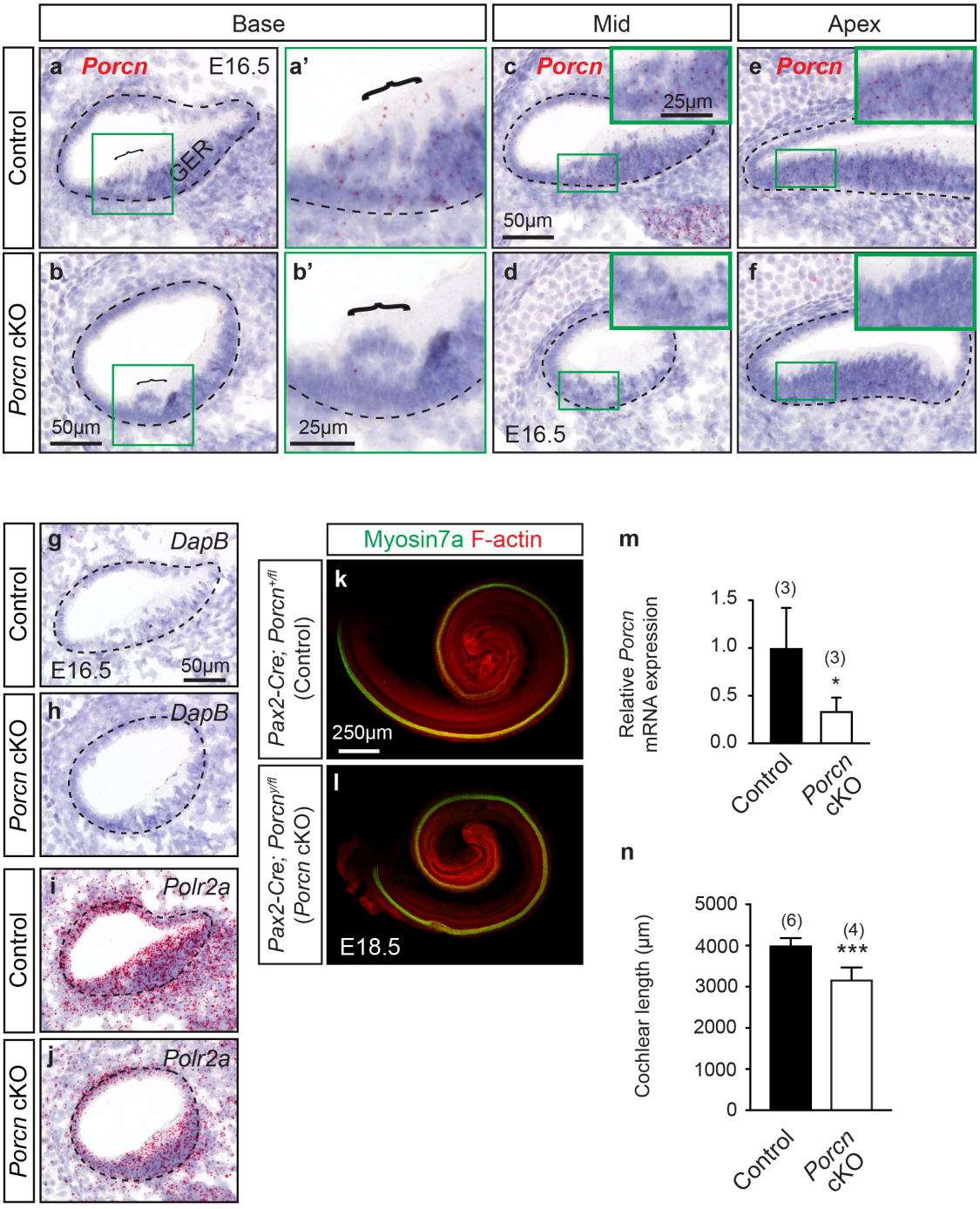

Figure S4. Genetic ablation of *Porcn* from the embryonic cochlear duct. (a-f) *In situ* hybridization (ISH) showing *Porcn* mRNA expression throughout the basal (a), middle (c) and apical (e) turns in sections of control (*Pax2*$^{Cre/+}$*; Porcn*$^{+/fl}$) cochleae. (a') high magnification image of the organ of Corti (brackets) showing *Porcn* mRNA expression. In contrast, *Porcn* mRNA signal was drastically reduced in each turn in *Porcn* cKO cochleae (*Pax2-Cre; Porcn*$^{fl/y}$) (b, d and f), including the organ of Corti (b'). Dashed lines highlight the cochlear duct. (g-j) ISH using negative (*DapB*) and positive (*Polr2a*) control probes in control (g and i) and *Porcn* cKO tissues (h and j). Hematoxylin was used as a counterstain in the ISH experiments. *In situ* probes that hybridize within the floxed exons 3-7 of *Porcn* were used. (k-l) Whole mounts of control (k) and *Porcn* cKO (l) cochleae labeled for Myosin7a (hair cells) and F-actin. *Porcn* cKO cochlea displayed hair cells but appeared dysmorphic and short. Detection for *Porcn* mRNA, Myosin7a and F-actin in control and *Porcn* cKO cochleae was repeated at least three times. (m) qPCR of *Porcn* mRNA showing a significant decrease in *Porcn* cKO cochleae relative to controls (n) *Porcn* cKO cochleae were significantly shorter than controls. Two-tailed t-test, * $P < 0.05$, ***$P < 0.001$. Data shown as mean±S.D. GER=Greater epithelial ridge.

Figure S5

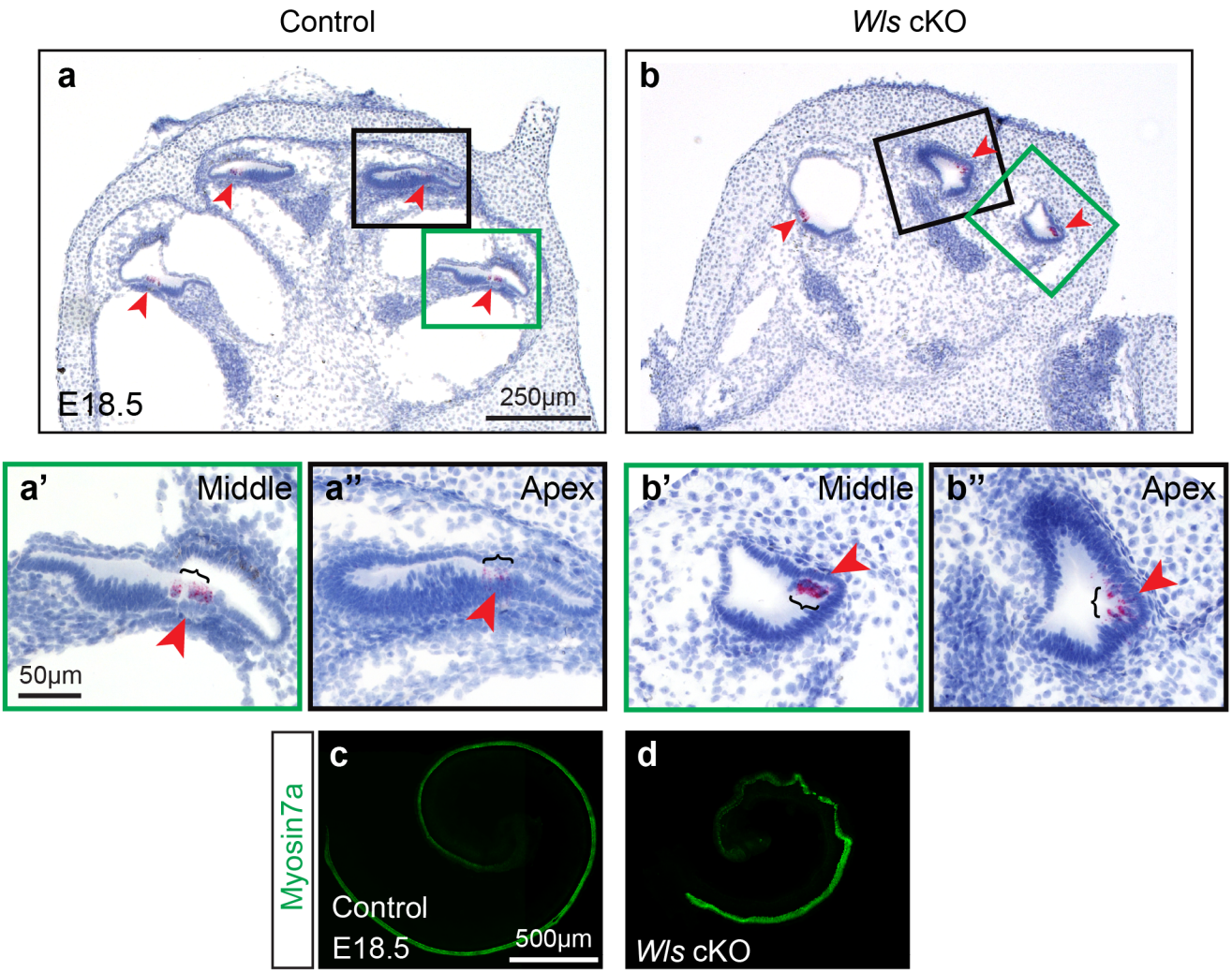

Figure S5. *Wls* is dispensable for hair cell specification. (a-b) *In situ* hybridization for *Atoh1* mRNA in sections of E18.5 control and *Wls* cKO cochleae. *Atoh1*-positive hair cells (red arrows) were found in each turn of E18.5 control cochlea. Middle (a') and apical (a'') turns shown. Though severely dysmorphic, *Wls* cKO cochleae similarly displayed *Atoh1*-positive hair cells. Middle (b') and apical (d'') turns shown. Brackets mark the organ of Corti. Sections were counterstained with hematoxylin (blue). (c-d) Immunostaining showing Myosin7a expression along the length of both control and *Wls* cKO cochleae (E18.5). *Wls* cKO cochleae appeared dysmorphic and short relative to controls. Each experiment was repeated at least three times.

Figure S6

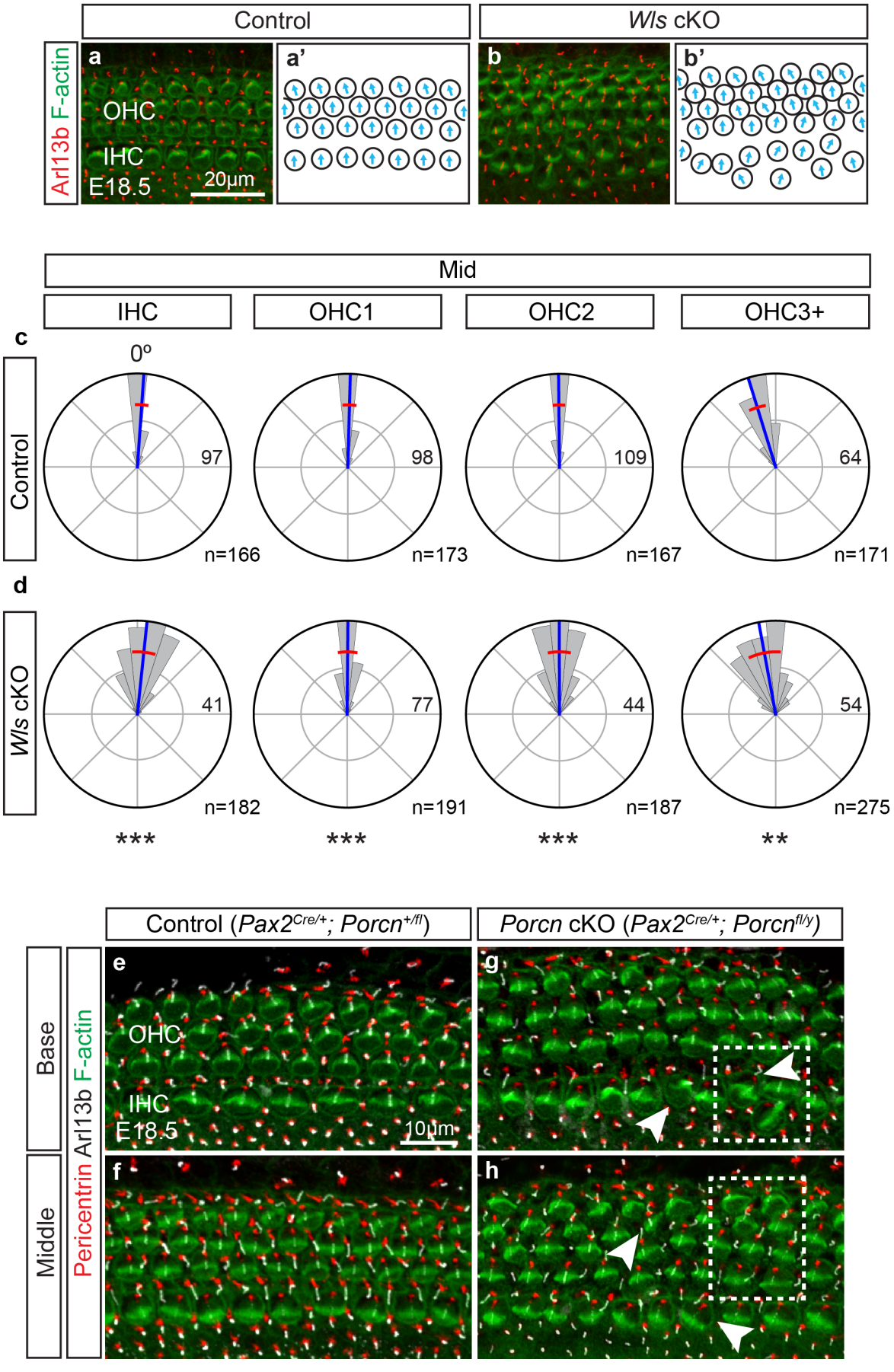

Figure S6. Bundle orientation defects in *Wls* and *Porcn* cKO cochleae. (a-b) E18.5 whole mount cochleae labeled for Arl13b (kinocilium) and F-actin (stereocilia bundles) (middle turn shown). Control cochleae displayed three rows of OHCs and one row of IHCs and stereocilia bundles arranged along the mediolateral axis of the cochlea. In contrast, *Wls* cKO cochleae exhibited supernumerary rows of OHCs and IHCs displaying stereocilia bundles deviated from the mediolateral axis. Panels (a') and (b') show the orientation of individual hair cells in control and *Wls* cKO cochleae, respectively. (c-d) Rose plots depicting the distribution and measurements of stereocilia bundle orientation in control and *Wls* cKO tissues. In comparison to each row of OHCs and IHCs in control cochleae, the variability in the stereocilia bundle orientation of HCs from the *Wls* cKO cochlea was significantly increased. The OHC3+ group included cells from the OHC3 row and OHCs more laterally located. Individual HCs were grouped and plotted into bins 15 degrees wide. The length of each petal represents the number of HCs therein, with the number of the longest petal (also the radius of the outer circle) stated. Radius of inner circle is half of the outer circle. Zero degrees designate the mediolateral axis. Circular mean and circular standard deviation shown in blue and red lines, respectively. (e-h) E18.5 control (*Pax2*$^{Cre/+}$*; Porcn*$^{+/fl}$) and *Porcn* cKO (*Pax2*$^{Cre/+}$*; Porcn*$^{fl/y}$) cochleae labeled for the basal body (Pericentrin), kinocilium (Arl13b), and F-actin (phalloidin). Basal body/kinocilium were localized to the lateral pole of hair cells in control cochleae and stereocilia bundles were aligned with the mediolateral axis. Basal (e) and middle (f) turns shown. (g-h) On the other hand, *Porcn* cKO cochlea displayed supernumerary IHCs and OHCs (dashed lines), and HCs with defective stereocilia bundle orientation and basal body/kinocilium positioning. Arrowheads mark misoriented HCs. Basal (g) and middle turns (h) shown. n=number of hair cells analyzed from 3 control and *Wls* cKO cochleae. Permutation test of equality of variances used. **p<0.01, ***p<0.001.

Figure S7

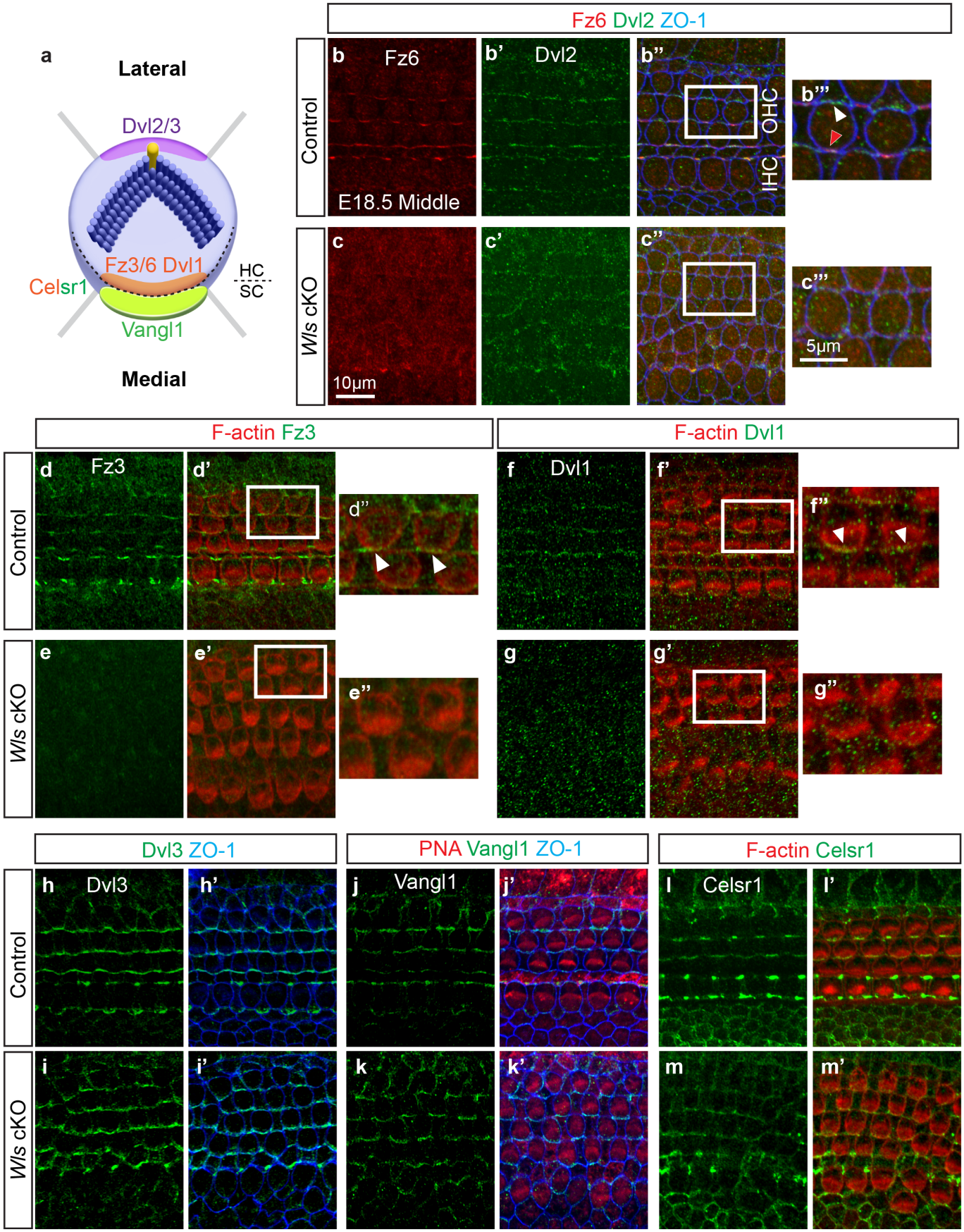

Figure S7. Aberrant localization of planar cell polarity core components in *Wls* cKO cochlea. (a) Cartoon depicting the asymmetric localization of core PCP proteins along the mediolateral axis of hair cells. (b) Representative images acquired from the middle turn of E18.5 control cochlea (*Emx2*$^{Cre/+}$; *Wls*$^{+/fl}$). Fz6 (red arrowhead) and Dvl2 (white arrowhead) were localized to the medial and lateral poles of hair cells (HCs), respectively. Co-staining with the cell junction protein ZO-1 (blue) is shown in panel (b''). (c) No asymmetric localization of Fz6 and Dvl2 was observed in HCs in *Wls* cKO cochlea (*Emx2*$^{Cre/+}$; *Wls*$^{fl/fl}$). Higher magnification of (b'') and (c'') are shown in (b''') and (c'''), respectively. (d) Control cochleae showed Fz3 (green, arrowheads) localized to the medial poles of F-actin-positive HCs. (e) In contrast, no asymmetric localization of Fz3 was observed in *Wls* cKO cochlea. Insets (white boxes) in control (d') and *Wls* cKO cochleae (e') are shown in (d'') and (e''), respectively. (f-g) In control cochlea, Dvl1 signal was mainly detected at the medial junctions of HCs with adjacent supporting cells (arrowheads). No asymmetric localization of Dvl1 was observed in HCs in *Wls* cKO. Higher magnification of insets in (f') and (g') are shown in (f'') and (g''), respectively. (h) Co-staining for Dvl3 with ZO-1 indicated localization of Dvl3 to the lateral side of HCs in both control and *Wls* cKO cochleae. (j-m) Comparable expression patterns of Vangl1 and Celsr1 were observed in both control and *Wls* cKO cochleae. Peanut agglutinin (PNA) and phalloidin marked F-actin-enriched HC bundles.

Figure S8

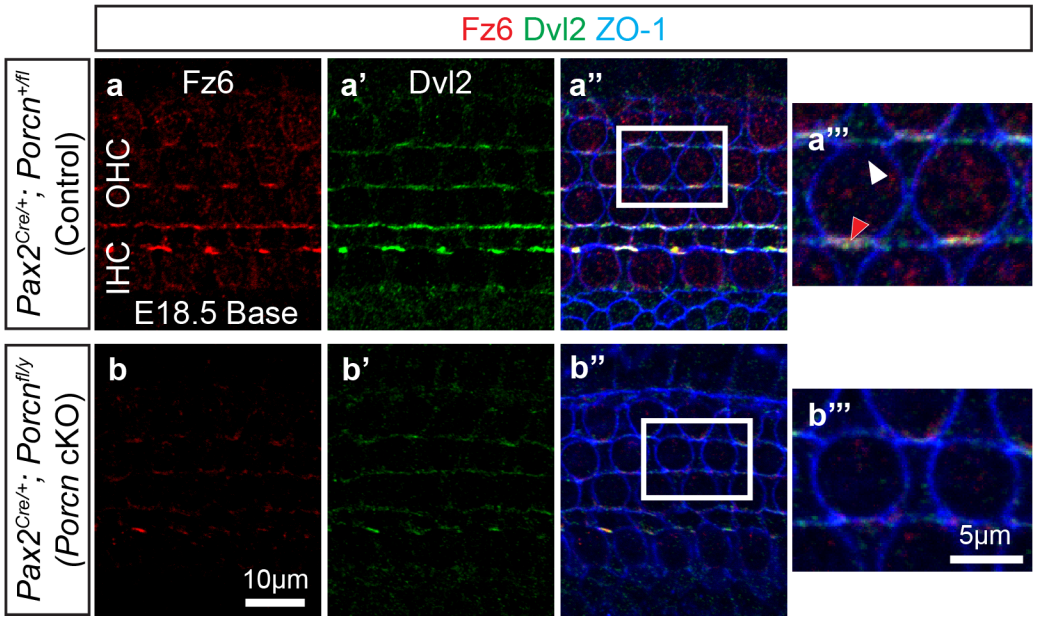

Figure S8. Abnormal localization of planar cell polarity core proteins in *Porcn* cKO cochlea. (a-b) Whole mount cochleae from E18.5 control (*Pax2*$^{Cre/+}$*; Porcn*$^{+/fl}$) and *Porcn* cKO (*Pax2*$^{Cre/+}$*; Porcn*$^{fl/y}$) mice immunostained for Fz6 (red), Dvl2 (green) and ZO-1 (blue). Control cochleae showed expression of Fz6 (red arrowhead) and Dvl2 (white arrowhead) restricted to the medial and lateral poles of HCs, respectively. In contrast, localized expression of Fz6 (b) and Dvl2 (b') was sharply decreased in *Porcn* cKO cochlea. High magnification images of insets (white boxes) in panels (a'') and (b'') are shown in (a''') and (b'''), respectively.

Figure S9

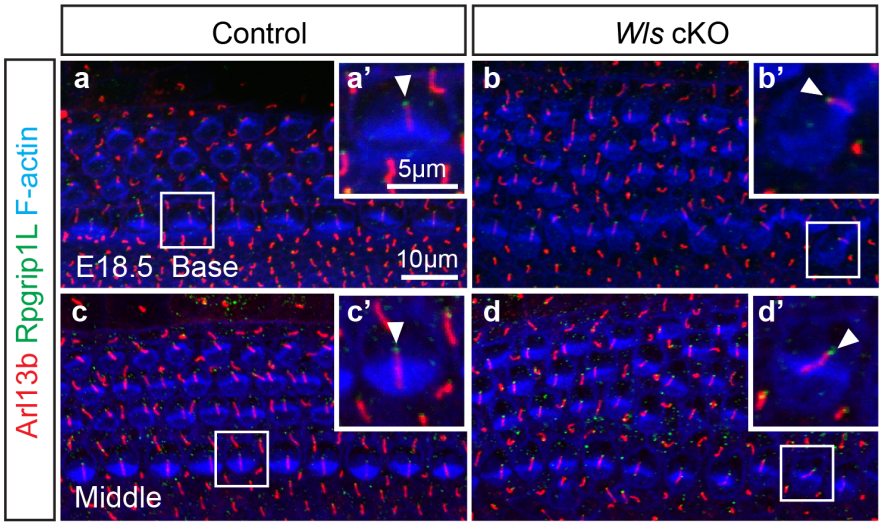

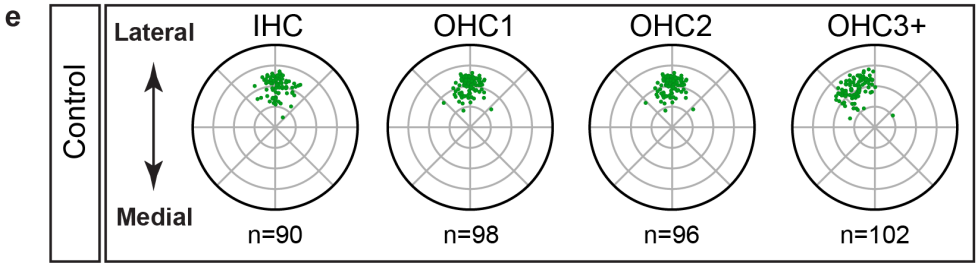

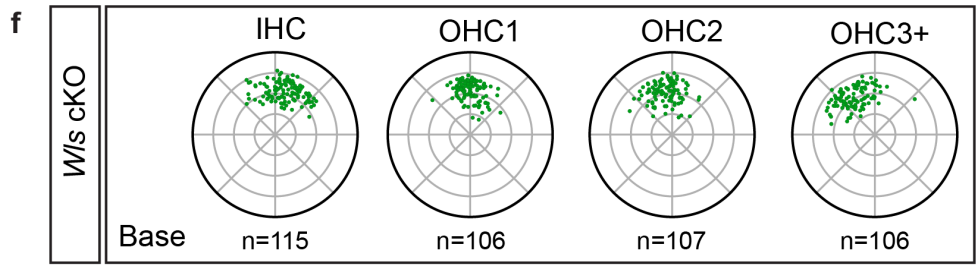

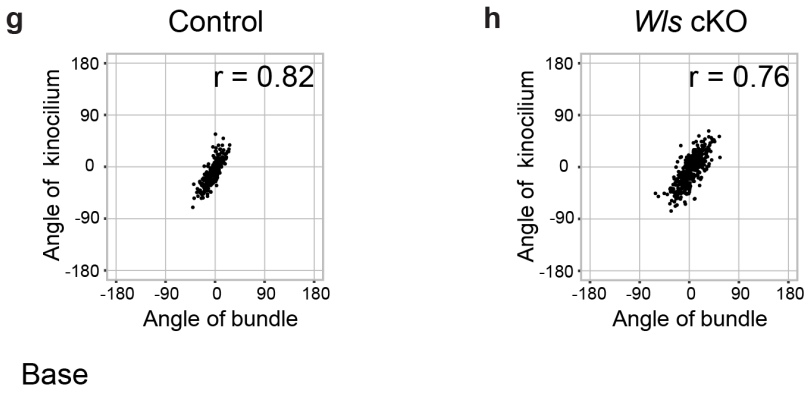

Figure S9. Aberrant kinocilium positioning in *Wls* cKO cochlea. (a-d) Cochlear whole mounts stained for Arl13b, Rpgrip1L and F-actin to label the kinocilium, transitional zone and stereocilia bundles, respectively. Basal and middle turns shown. In control cochlea (*Emx2*$^{Cre/+}$*; Wls*$^{+/fl}$), both Arl13b and Rpgrip1L (arrowheads) were located at the lateral pole of OHCs and IHCs and stereociliary bundles were uniformly oriented along the mediolateral axis. In contrast, *Wls* cKO (*Emx2*$^{Cre/+}$*; Wls*$^{fl/fl}$) tissues showed malpositioned kinocilium (arrowheads) and misoriented stereocilia bundles (b and d). Higher magnifications of insets (white boxes) in (a-d) are shown in (a'-d'). (e) Scatter plots of kinocilium position (based on Rpgrip1L expression) in hair cells from basal turn of E18.5 control cochlea. Kinocilium positions were tightly clustered at the lateral pole of each row of hair cells. (f) In *Wls* cKO cochlea, the kinocilium position was more scattered in comparison to controls. The OHC3+ group included cells from the OHC3 row and OHCs more laterally located. In the scatter plots, concentric circles indicate relative distance from the center of the apical surface of HCs. n=HC number analyzed from 3 control and *Wls* cKO cochleae. (g-h) The angular position of kinocilium and the angle of stereocilia bundle orientation were highly correlated in both control ($Pearson_{circular}$ correlation test, r=0.82, n=386, p<0.001) and *Wls* cKO cochleae ($Pearson_{circular}$ correlation test, r =0.76, n=434, p<0.001).

Figure S10

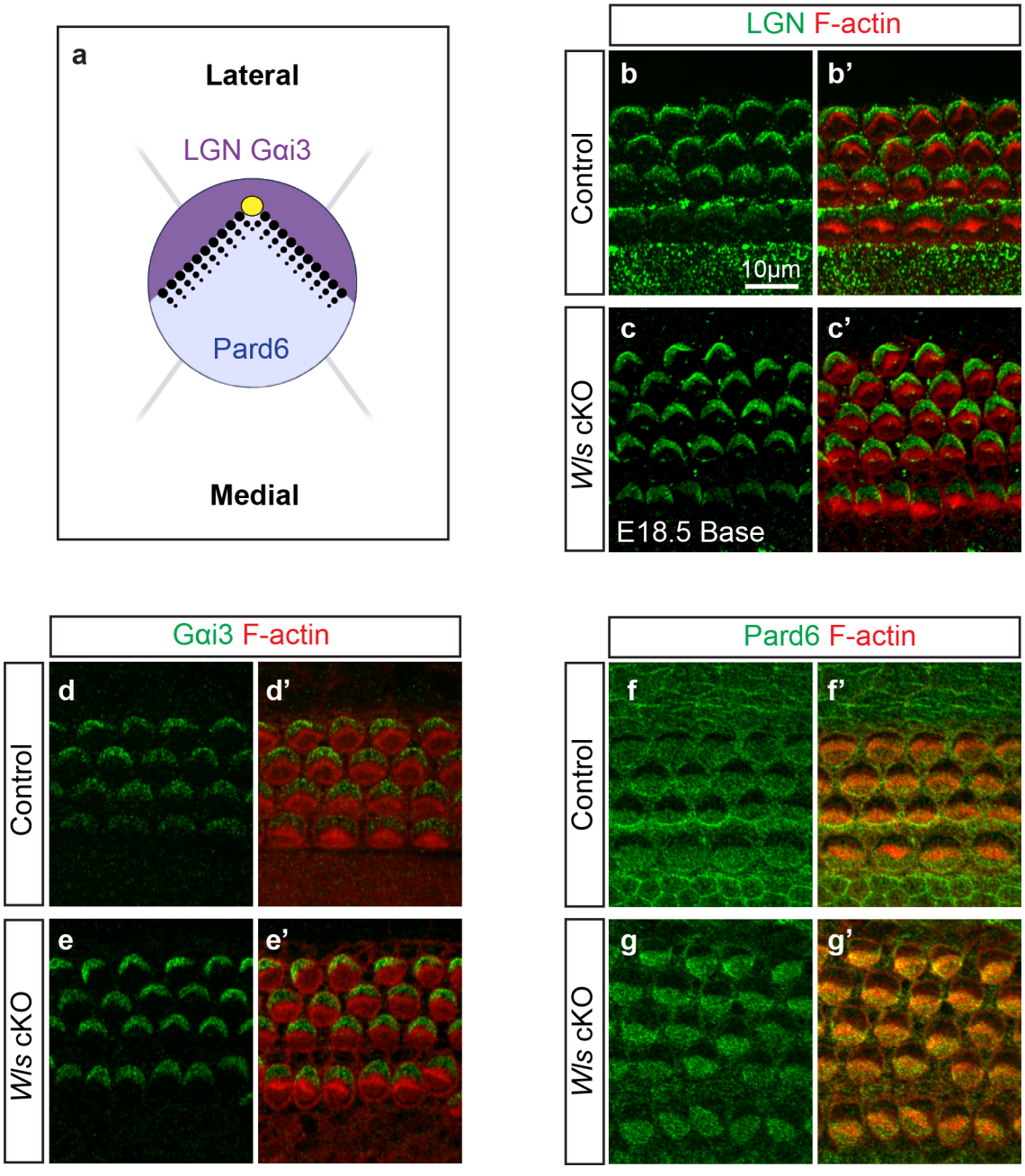

Figure S10. *Wls* is dispensable for the asymmetric distribution of intrinsic polarity proteins. (a) Cartoon depicting the asymmetric distribution of intrinsic polarity proteins in the apical surface of HCs. LGN and Gαi3 are both located on the lateral side and Pard6 on the medial side of hair cells. (b-c) In control (*Emx2*$^{Cre/+}$*; Wls*$^{+/fl}$) and *Wls* cKO (*Emx2*$^{Cre/+}$*; Wls*$^{fl/fl}$) cochleae (basal turn, E18.5), LGN (green) was present in the lateral side of hair cells. Bundles were stained for F-actin (red). (d-e) Gαi3 was found localized to the lateral side of HCs in both control and *Wls* cKO tissues. (f-g) Pard6 was localized to the medial side of HCs in both control and *Wls* cKO cochleae.

Figure S11

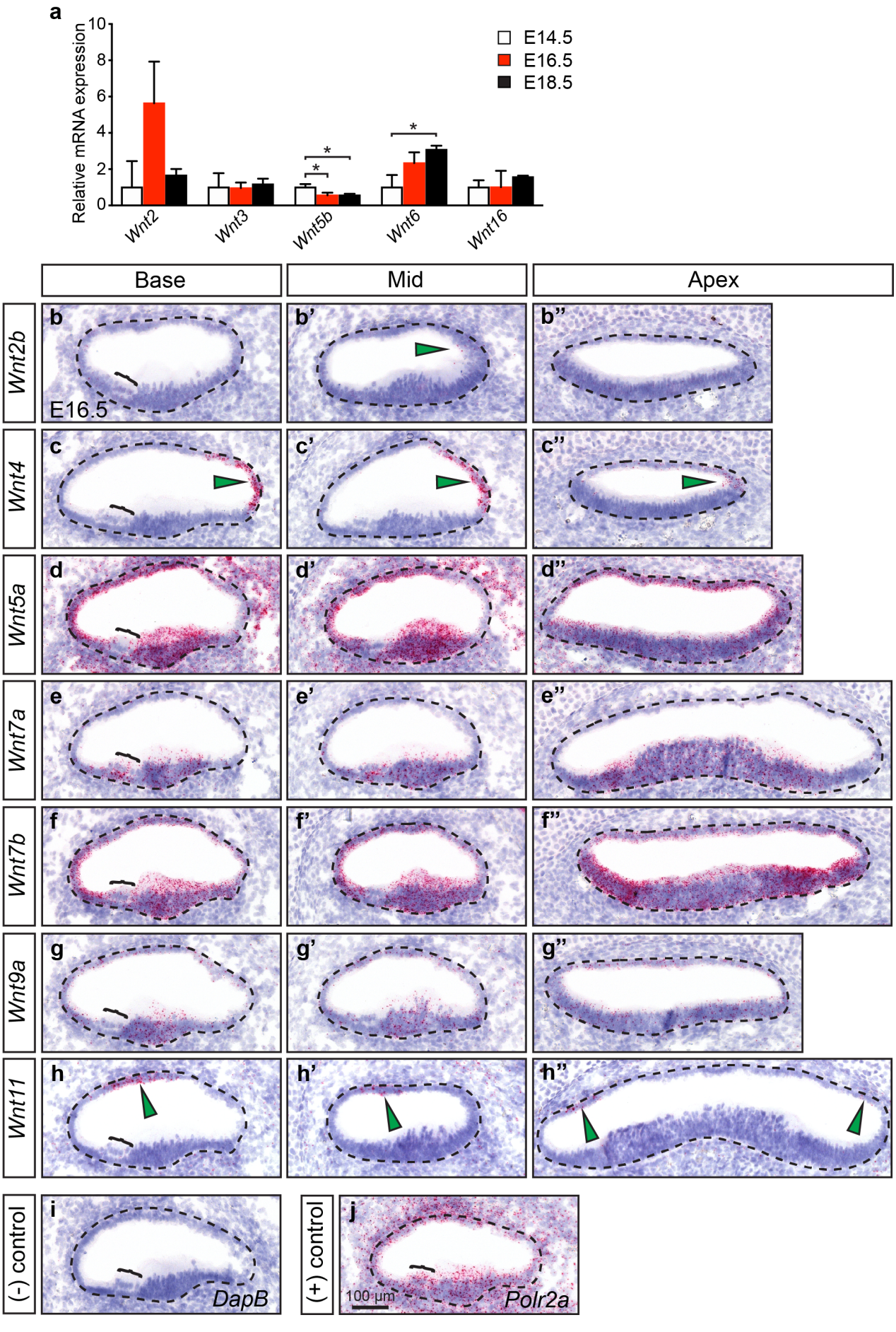

Figure S11. Expression of Wnt ligands in E16.5 cochlear duct. (a) qPCR of Wnt ligands during cochlear development. n=3 for each age group. (b-b'') *In situ* hybridization detecting a low level of *Wnt2b* mRNA in the medial aspect of the cochlear duct (marked by dashed line) in the middle turn. (c-c'') A distinct *Wnt4* expression domain was observed in the medial cochlear roof, most notably in the basal and middle turns. (d-d'') *Wnt5a* was robustly expressed throughout the cochlear duct. (e-e'') *Wnt7a* mRNA was mostly detected in the cochlear floor, whereas *Wnt7b* mRNA (f-f'') was expressed throughout the cochlear duct. (g-g'') A low level of *Wnt9a* expression was noted throughout the cochlear duct. (h-h'') *Wnt11* expression was found in the roof of the cochlea, most notably in the basal turn. (i-j) *DapB* and *Polr2a* were used as negative and positive control probes, respectively. In addition, hematoxylin (blue) was used as counterstain. Arrowheads highlight mRNA signals, whereas brackets indicate the organ of Corti. Each experiment was repeated at least three times. Two-tailed Student's t-test. *P<0.05. Data shown as mean±S.D.

Figure S12

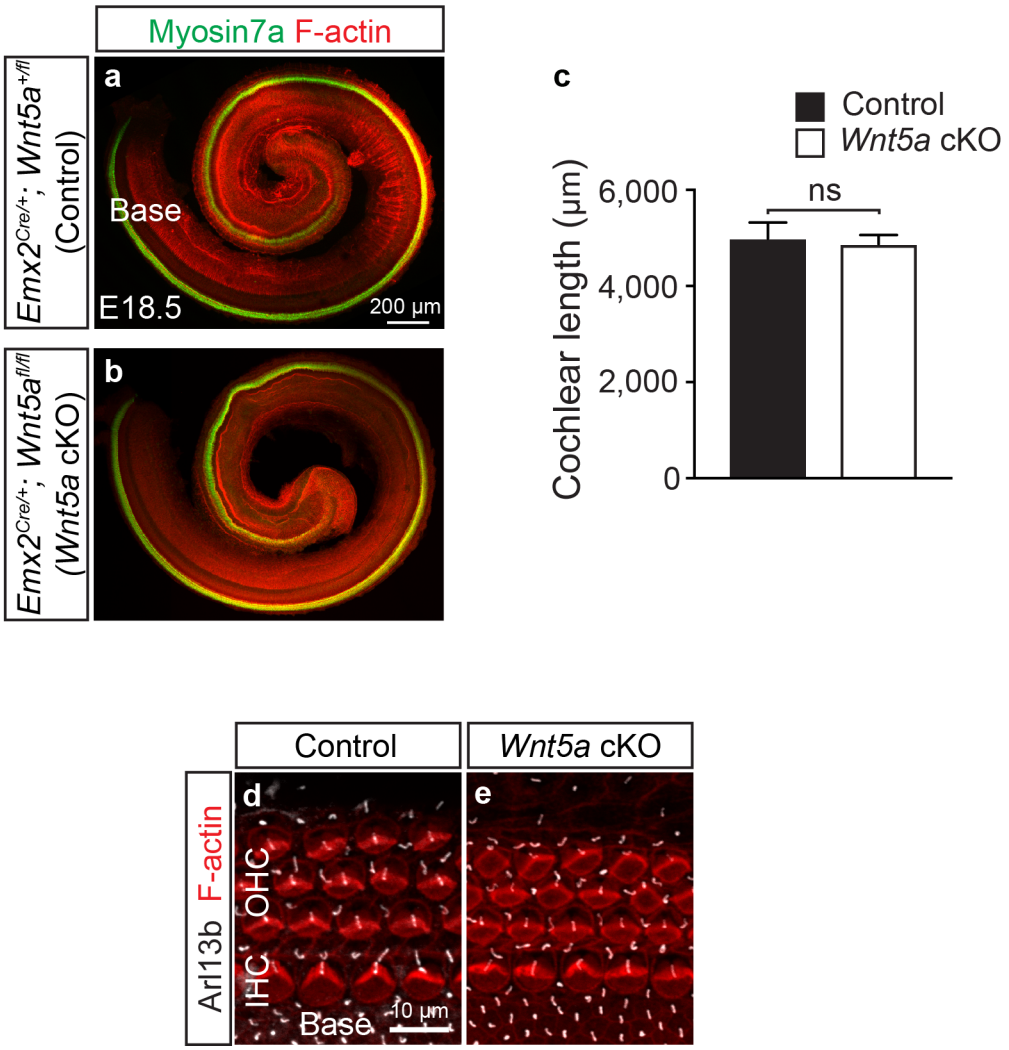

Figure S12. Genetic ablation of *Wnt5a* from the cochlear duct. (a-b) E18.5 whole cochlear mounts stained for Myosin7a (green, hair cells) and F-actin (red). In comparison to controls (*Emx2*$^{Cre/+}$*; Wnt5a*$^{+/fl}$), *Wnt5a* cKO (*Emx2*$^{Cre/+}$*; Wnt5a*$^{fl/fl}$) cochleae showed no gross disorganization of HCs or decrease in length. (c) No significant differences in length were observed between *Wnt5a* cKO and control cochleae. n=3 per each genotype. (d-e) Both control and *Wnt5a* cKO tissues displayed three rows of OHCs and one row of IHCs. No misorientation of stereocilia bundles or mislocalization of Arl13b-labeled kinocilium was noted in the *Wnt5a* cKO cochleae. Student's t-test used, ns= not significant. Data shown as mean±S.D.

Figure S13

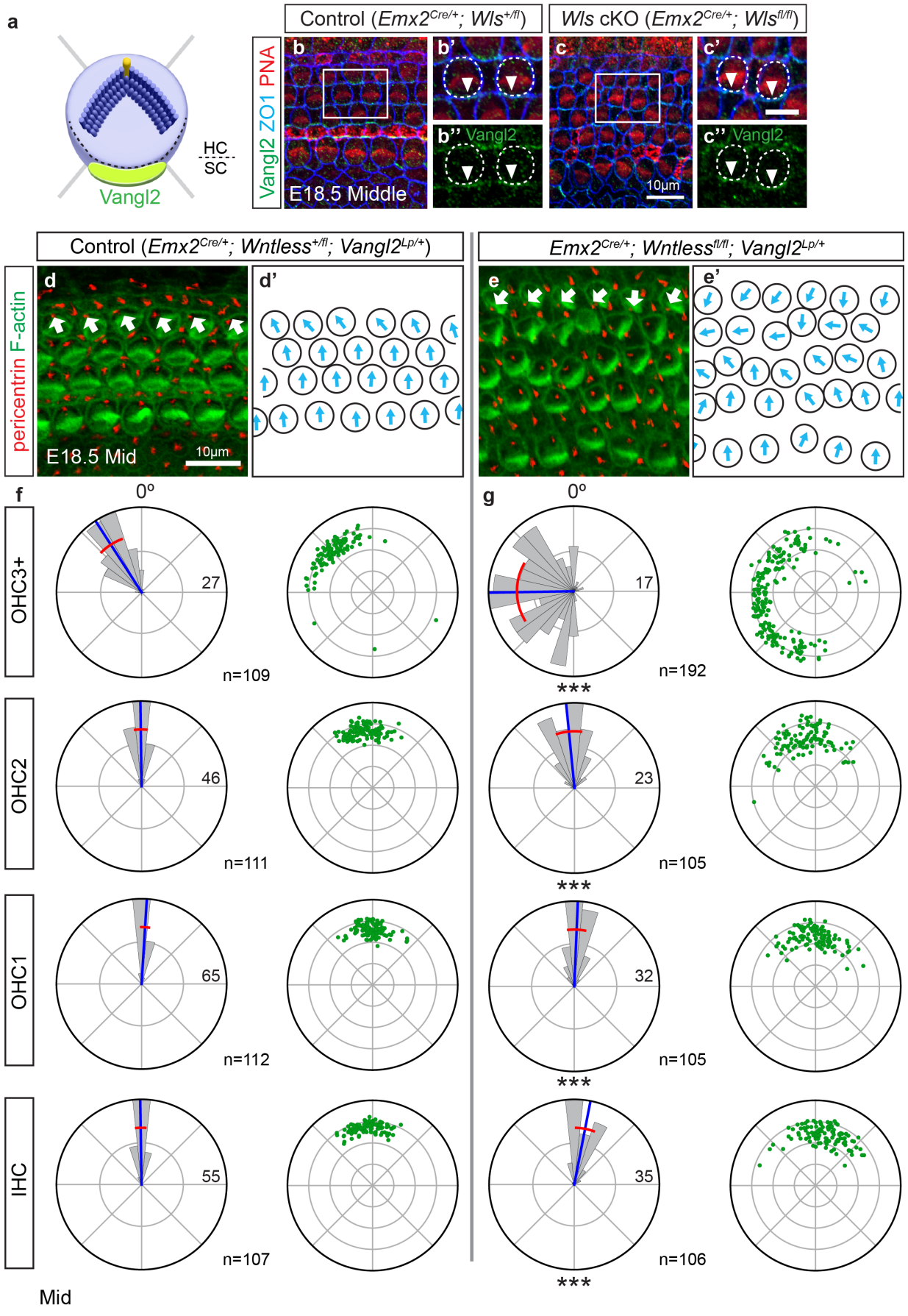

Figure S13. *Vangl2* genetically interacts with *Wls* to regulate PCP. (a) Schematic illustrating the asymmetric localization of Vangl2 (green) at the lateral side of supporting cells. (b-c) Vangl2 was asymmetrically localized in both control (*Emx2*$^{Cre/+}$*; Wls*$^{+/fl}$) and *Wls* cKO (*Emx2*$^{Cre/+}$*; Wls*$^{fl/fl}$) cochleae. ZO-1 and PNA mark tight junctions and stereocilia bundles, respectively. All the images correspond to the middle turn of the cochlea. High magnification images showing Vangl2 expression in control (b' and b'') and *Wls* cKO tissues (c' and c''). Dashed circles demark cell boundaries and white arrowheads highlight Vangl2 immunolocalization. (d-e) E18.5 cochleae were double stained for Pericentrin (red) and F-actin (green) to label basal bodies and stereocilia bundles in HCs, respectively. (d) In control (*Emx2*$^{Cre/+}$*; Wls*$^{+/fl}$*; Vangl2*$^{Lp/+}$), bundle orientation and basal body positioning appeared normal for IHCs and OHCs. No extranumerary HCs were observed in control cochlea (d and d'). (e) In contrast, *Wls cKO; Vangl2*$^{Lp/+}$ (*Emx2*$^{Cre/+}$*; Wls*$^{fl/fl}$*; Vangl2*$^{Lp/+}$) cochlea displayed many misoriented stereocilia bundles and malpositioned basal bodies (arrows). In addition, extranumerary OHCs were observed in these tissues. In (d) and (e), arrows indicate stereocilia bundle orientations. (d'-e') illustrate the orientation of stereocilia bundles from individual HCs in panels (d-e), respectively. (f-g) Rose and scatter plots depicting the distribution of stereocilia bundle orientation and basal body positioning, respectively. (f) In control, HCs displayed stereocilia bundles aligned in the mediolateral axis and tightly clustered basal bodies at the lateral pole. The third row of OHCs were consistently rotated minus 30 degrees along the mediolateral axis of the cochlea (towards the apex) and with their basal bodies clustered at that angle. In contrast, in *Wls cKO; Vangl2*$^{Lp/+}$ cochleae, HCs showed significantly more variable bundle orientation, particularly among the outermost row of OHCs (Permutation test of equality of variances, $p<0.001$).

Moreover, basal body positioning in *Wls cKO; Vangl2*$^{Lp/+}$ cochleae was more scattered than in control, particularly in the most lateral outer hair cells. The OHC3+ group included cells from the OHC3 row plus more laterally located OHCs. In the scatter plots, concentric circles indicate relative distance from the center of the apical surface of HCs. n=number of hair cells analyzed from 3 control and *Wls cKO; Vangl2*$^{Lp/+}$ cochleae. Zero degrees designate the mediolateral axis. Permutation test of equality of variances used. ***p<0.001. Circular mean and circular standard deviation shown in blue and red lines, respectively.

Figure S14

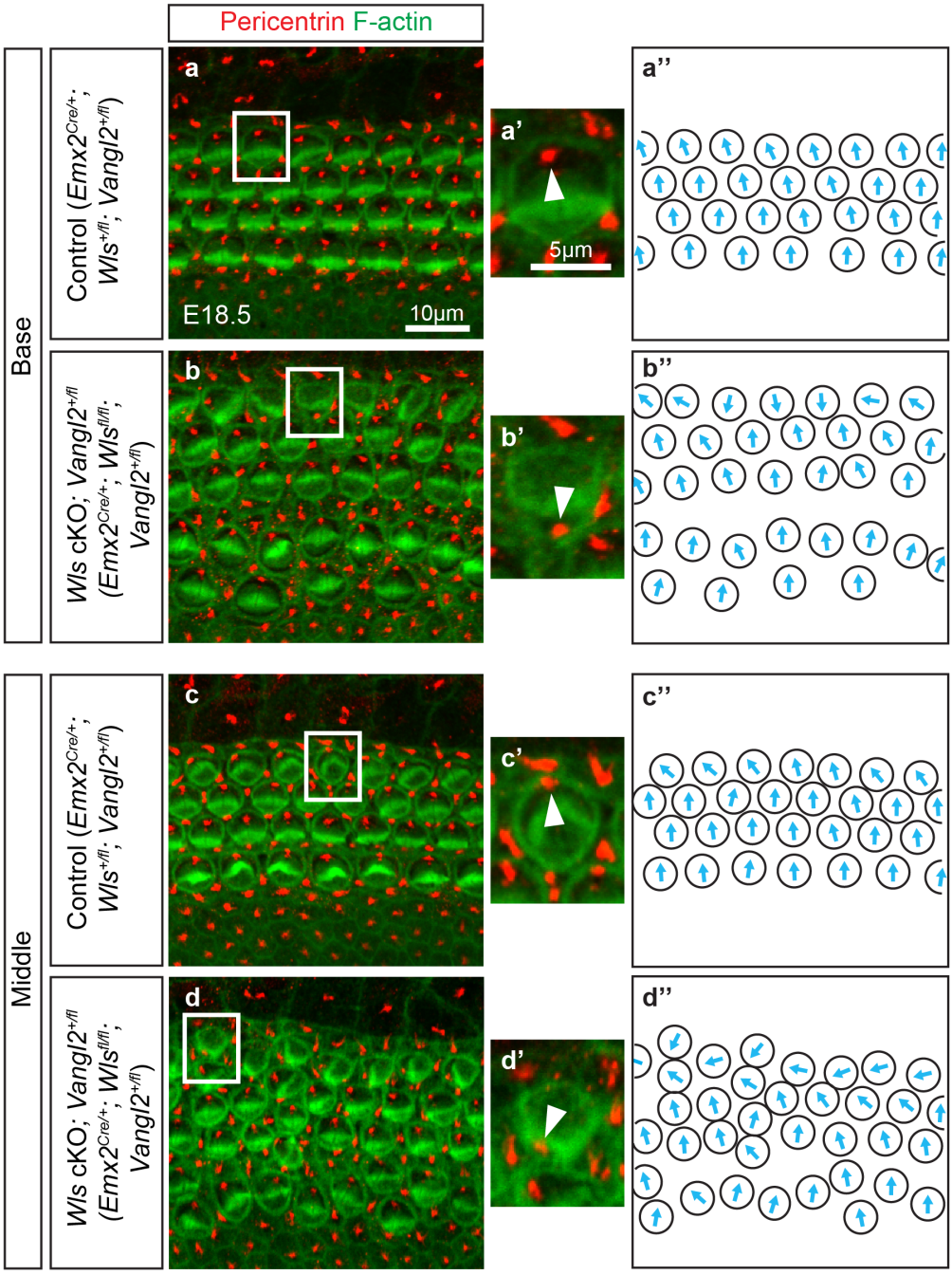

Figure S14. *Vangl2* and *Wls* coordinate to regulate planar polarization. (a-d) Pericentrin (red) and F-actin (green) marked the basal body and stereocilia bundles, respectively, in cochleae from E18.5 control (*Emx2*$^{Cre/+}$*; Wls*$^{+/fl}$*; Vangl2*$^{+/fl}$) and *Wls* cKO*; Vangl2*$^{+/fl}$ (*Emx2*$^{Cre/+}$*; Wls*$^{fl/fl}$*; Vangl2*$^{+/fl}$) animals. Basal and middle turns shown. (a, c) In the control cochleae, stereocilia bundles were uniformly oriented along the mediolateral axis and basal bodies (arrowheads) were mainly located at the lateral pole of hair cells (HCs). There were also no extranumerary HCs. (b, d) In contrast, HCs in *Wls cKO; Vangl2*$^{+/fl}$ cochleae showed misoriented bundles along with basal body positioning defects, which were most severe in the outermost row of OHCs. Some OHCs were rotated almost 180 degrees with respect to the mediolateral axis. In addition, extranumerary IHCs and OHCs were observed in *Wls* cKO*; Vangl2*$^{+/fl}$ cochleae. Insets (white boxes) in control and *Wls* cKO*; Vangl2*$^{+/fl}$ tissues are shown in panels (a', c') and (b', d'), respectively. Arrowheads mark the position of basal bodies. For panels (a-d), the orientation of each hair cell is illustrated in (a''-d''), respectively. Three control and *Wls* cKO*; Vangl2*$^{+/fl}$ cochleae were analyzed.

Table S1. qPCR primer sequences

Gene Name	Forward primer (5' -> 3')	Reverse primer (5' -> 3')	Accession number
Wnt1	CAA ATG GCA ATT CCG AAA CCG	GGA GGT GAT TGC GAA GAT GA	NM_021279.4
Wnt2	GTA GAT GCC AAG GAG AGG AAA G	CAC ACC ATG ACA CTT GCA TTC	NM_023653.5
Wnt2b	CTC ATG AAC TTA CAC AAC AAC CG	CAG AGT ACA GGA GCC ACT CA	NM_009520.3
Wnt3	AGC TGC CAA GAG TGT ATT CG	CAT GGG ACT TCG ATG AAT GGA	NM_009521.2
Wnt3a	ATC TTT GGC CCT GTT CTG G	GAG CGT GTC ACT GCG AA	NM_009522.2
Wnt4	GGC ACT CAT GAA TCT TCA CAA C	GCA CGT CTT TAC CTC GCA	NM_009523.2
Wnt5a	GTG CCA TGT CTT CCA AGT TCT	GTT ATT CAT ACC TAG AGA CCA CCA	NM_009524.3
Wnt5b	CCA ACA CCA GTT TCG ACA GA	AAG GCA GTC TCT CGG CTA	NM_009525.3
Wnt6	GTT CCA GTT CCG TTT CCG A	ATG GAA CAG GCT TGA GTG AC	NM_009526.3
Wnt7a	CAG TTT CAG TTC CGA AAT GGC	GAT AAT CGC ATA GGT GAA GGC A	NM_009527.3
Wnt7b	CCA GCA CCA GTT CCG ATT	CCG TGA TGG CAT AGG TGA A	NM_009528.3
Wnt8a	CAG ACT CTT CGT GGA CAG TT	CCT GAG ATG CCA TGA CAC TT	NM_009290.2
Wnt8b	TGT GCG TTC TTC TAG TCA CTT G	GTA GAC CAG GTA AGC CTT TGG	NM_011720.3
Wnt9a	CAG TAC CAG TTC CGC TTT GAG	GAA GAG ATG GCG TAG AGG AAA	NM_139298.2
Wnt9b	AAG TAC AGC ACC AAG TTC CTC	CAC TTG CAG GTT GTT CTC AG	NM_011719.4
Wnt10a	CTC CTG TTC TTC CTA CTG CTG	ACT GTG TTG GCG TTG AGC	NM_009518.2
Wnt10b	GAT CCT GCA CCT GAA CCG	CCG ACT GAA CAA AGC CAA GA	NM_011718.2
Wnt11	ATG AAG AAT GAG AAG GTG GGA T	GTA CTT GCA GTG ACA TCG CT	NM_001285792.1
Wnt16	GGA ACC CAG GGC AAC TG	CTC TTG CAC AGC TCC TTC TG	NM_053116.4
Wls	TTT CCA AAT CGT TGC CTT TCT G	TGG TTC TTA CGG ACA TCC AC	NM_026582(2)
Porcn	TCC GTC ACC ATC CTC ATC TAC	GAG ACA CCG CCT TCA TGG	NM_016913(4)
Rpl19	GGTCTGGTTGGATCCCAATG	CCCGGGAATGGACAGTCA	NM_009078.2

Table S2. Antibody list.

Protein	Antibody	Source	Dilution
Wls	EUR302	Kerafast	1:10000
Wls	17950-1-AP	Proteintech	1:500
Vangl2	21492-1-AP	Proteintech	1:250
Vangl1	HPA025235	Sigma-Aldrich	1:1000
Fzd6	AF1526	R and D Systems	1:250
Fzd3		gift from Jeremy Nathans	1:500
Celsr1		gift from Elaine Fuchs	1:3000
Dvl1	27384-1-AP	Proteintech	1:250
Dvl2	3224	Cell Signaling Technology	1:250
Dvl2	12037-1-AP	Proteintech	1:250
Dvl3	13444-1-AP	Proteintech	1:1000
Atoh1	21215-1-AP	Proteintech	1:1000
Myo7a	25-6790	Proteus Biosciences	1:1000
Sox2	sc-17320	Santa Cruz	1:200
ZO-1	33-9100	Thermo Scientific	1:1000
Arl13b	75-287	NeuroMab	1:500
Pericentrin	923701	BioLegend	1:1000
Acetylated α-tubulin	T7451	Sigma-Aldrich	1:500
RpGrip1L	55160-1-AP	Proteintech	1:500
Gnαi3	11641-1-AP	Proteintech	1:250
Lgn		gift from Quansheng Du	1:1000
ParD6B	13996-1-AP	Proteintech	1:250